
A Modeling Analysis of Monoclonal Antibody Percolation Through Tumors: A Binding-Site Barrier

Kenji Fujimori*, David G. Covell, John E. Fletcher, and John N. Weinstein

Laboratory of Mathematical Biology, Division of Cancer Biology and Diagnosis, National Cancer Institute; and Laboratory of Applied Studies, Division of Computer Research and Technology, National Institutes of Health, Bethesda, Maryland

For successful use of radiolabeled monoclonal antibodies (MAbs) for diagnosis and therapy, it is helpful to understand both global and microscopic aspects of antibody biodistribution. In this study, antibody distribution in a tumor is simulated by splicing together information on global pharmacokinetics: transport across the capillary wall, diffusive penetration through the tumor interstitial space, and antigen-antibody interaction. The geometry simulated corresponds to spherical nodules of densely packed tumor cells. This modeling analysis demonstrates that: 1) antigen-antibody binding in tumors can retard antibody percolation; 2) high antibody affinity at a given dose tends to decrease antibody percolation because there are fewer free antibody molecules. The result is a more heterogeneous distribution; 3) the average antibody concentration in the tumor does not increase linearly with affinity; and 4) increasing antibody dose leads to better percolation and more uniform distribution. This mathematical model and the general principles developed here can be applied as well to other biologic ligands.

J Nucl Med 1990; 31:1191-1198

Understanding the global and microscopic pharmacology of monoclonal antibodies (MAbs) may improve the efficacy of radioimmunodetection and radioimmunotherapy of tumors. Recently, many authors have reported that heterogeneous MAb distribution in tumors degrades the efficacy (1-5). Part of that heterogeneity arises from nonuniform distribution of antigen among tumor cells and among regions of a tumor (6,7); another part may be explained by heterogeneous tumor blood supply (8,9). In addition to these factors, the observation that MAb tends to accumulate in the

tumor interstitium adjacent to capillary walls (3), despite favorable interstitial transport characteristics of tumors, suggests that there may be a barrier to MAb penetration far from the capillaries.

For the last several years, we have been trying to understand the global pharmacology of MAb in humans (10) and in other animals (11,12). For further understanding of MAb distribution in the tumor, one must consider as well the microscopic pharmacology: transport across the capillary wall, transport in tumor interstitium, cellular binding, and metabolism. From that perspective, the global pharmacology can be viewed as an input to the microscopic problem. Plasma profiles determine what concentration of MAb is available at each point in time to cross the capillary wall and percolate through the extravascular space to reach antigens there. The next question: how high and how uniform will the concentration of MAb be as a function of time and as a function of various parameters of the system? To study the question of access to tumor antigen by MAb, we have developed a set of mathematic models based on the global and microscopic parameters. Here we use these models to examine the relationship between affinity and microscopic MAb distribution.

Our aim here is to provide an aid to concept development and a guide to further experiment rather than to fit particular data sets. A central consideration is what we have termed the "binding-site barrier"—the prediction that bindable antibody will be retarded in its transport through the tumor interstitial space by the very fact of its successful binding to antigen on the tumor cell surface near entry points. Although parameter values for IgG are used here for illustrative calculations, the model is quite general and can also treat immunoglobulin types of other molecular weight and valence (e.g., IgM), their fragments (e.g., F(ab')₂, Fab), and other biologic ligands. Basic principles of the binding-site barrier problem remain essentially the same for these other macromolecules. Early stages of this work have been described in preliminary form elsewhere (13-

Received Sept. 14, 1989; revision accepted Jan. 23, 1990.

For reprints contact: Kenji Fujimori, MD, Building 10, Room 4B-56, NIH, The Laboratory of Mathematical Biology, National Cancer Institute, 9000 Rockville Pike, Bethesda, MD 20892.

* Permanent address: Department of Nuclear Medicine, School of Medicine, Hokkaido University, Sapporo, Japan.

16), and we have also analyzed a cylindrical model in which antibody flows radially from a central vessel through a cord of tumor cells (17). Here, we represent the tumor by spheroids of cells, through which antibody penetrates toward the center. This geometry most directly resembles that of the nodular lymphomas, but it pertains in a general way to other histologies as well.

MATERIALS AND METHODS

Global Pharmacokinetics

The global pharmacokinetics of MAb following intravenous (i.v.) injection were simulated by biexponential fits, using standard proportionally-weighted, least-squares techniques. Data for curve fitting were based on clinical studies of indium-111- (^{111}In) labeled 9.2.27 (IgG_{2a}, directed against a Mr 250,000 glycoprotein/proteoglycan expressed on melanoma cells) in melanoma patients (10). Those parameter values were used for simulating the plasma MAb concentration in blood capillaries, including those of the tumor. The plasma pharmacokinetics were assumed to be independent of MAb binding to tumor. The values were taken as representative for IgG, although there is clearly considerable variation in the numbers obtained from various clinical studies.

MAb Percolation

A spherical model was constructed for simulating a small nodule in the tumor. In this model, antibody percolates from the surface of the nodule toward the center (Fig. 1). The nodule diameter was taken as 300 μm so that it does not contain a necrotic center. Although the effective diameter of cell nodules may vary among and within tumors (18), the basic principle of analysis remains essentially the same.

The spherical nodule of radius $R = 150 \mu\text{m}$ is divided into N (set as $N = 30$ in this study) thin concentric spherical shells, each at radial position r_i (for $i = 1, \dots, N$). Radially symmetric

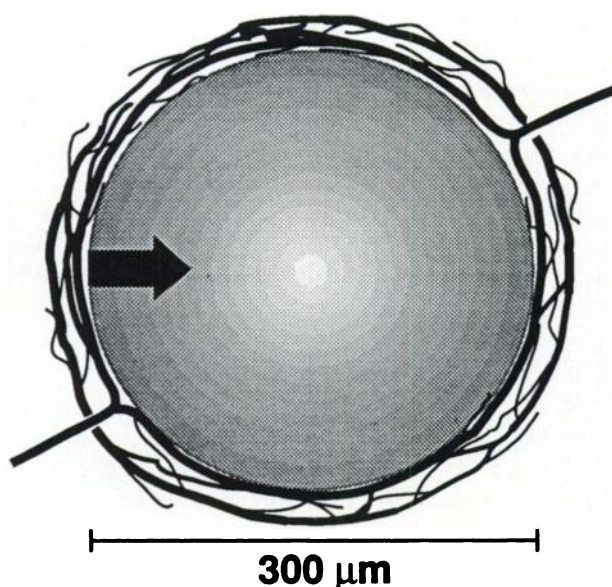


FIGURE 1

A cut-away schematic of the spherical model. The sphere diameter is taken as 300 μm . MAbs percolate from the nodule's surface toward the center.

diffusion in a sphere is governed by the following pair of differential equations for free MAb and immobile, unoccupied antigen at position i (19):

$$\frac{\partial c_i}{\partial t} = D \left(\frac{\partial^2 c_i}{\partial r^2} \Big|_{r=r_i} - \frac{2}{R-r_i} \frac{\partial c_i}{\partial r} \Big|_{r=r_i} \right) - k_f c_i s_i + k_r \bar{c} s_i \quad (1a)$$

$$\frac{ds_i}{dt} = -n k_f c_i s_i + n k_r \bar{c} s_i \quad (1b)$$

where c_i is the concentration of free MAb (M); s_i is the concentration of free antigen (M); $\bar{c} s_i$ is the concentration of bound MAb (M); k_f is the forward rate constant for specific binding ($\text{M}^{-1}\text{s}^{-1}$); k_r is the corresponding reverse rate constant (s^{-1}); D is the effective interstitial diffusion coefficient (cm^2/s); R is the radius of the nodule (μm); r_i is the radial distance from the surface of the nodule (μm); and n is the valence of the MAb (for IgG, $n = 2$). D , k_f , and k_r are assumed to be constant throughout the space. The nodule is taken to be radially symmetrical, and there is assumed to be no convection within it. We have chosen to consider here the simple case in which binding of MAb is assumed to be completely bivalent. More generally, if monovalent and bivalent binding were to be represented explicitly, Equation 1b would be replaced by two ordinary differential equations for the sequential binding steps. However, not enough information is currently available on the binding characteristics of tumor antigens to justify the more general formulation. The total concentration of binding sites s_0 (uniform throughout the tumor) is given by the expression:

$$s_0 = s_i + n \bar{c} s_i \quad (2)$$

It is assumed that the blood supply is constrained to the nodule surface (20) and that branch vessels which penetrate nodules are functionally negligible (9). It is also assumed that the stroma surrounding the nodule has no appreciable volume but allows free penetration of MAb from the capillary to the surface of the nodule. This model most clearly resembles the histology of nodular lymphomas and pre-vascular tumor nodules. Although the actual microscopic geometries of other neoplasms may differ, many of the same principles are expected to apply qualitatively to them as well. The model also applied to incubation of tumor spheroids in vitro. In that case, however, the capillary permeation coefficient would be considered as infinite, and the external MAb concentration would be taken as constant. Langmuir et al. have used autoradiography to study the distribution of radiolabeled-MAb in such spheroids (21). McFadden and Kwok have analyzed penetration of MAb into spheroids, using a mathematical model with non-saturable binding (22).

MAb transport (J_s , $\text{cm} \cdot \text{M}/\text{s}$) across the capillary wall is governed by (23):

$$J_s \approx P_{eff}(c_p - c_i) \quad (3)$$

where P_{eff} is the effective capillary permeation constant (cm/s), c_p is MAb concentration in plasma (M), and c_i is free MAb concentration in the nodule adjacent to the surface (M). The relationship of P_{eff} to diffusive and convective transport across the capillary walls is discussed in detail elsewhere (17).

The boundary condition at the surface of the nodule is obtained by equating MAb flux through the capillary wall and

MAB transport in tumor adjacent to the surface (17):

$$P_{eff}(c_p - c_i) = D \frac{\partial c_i}{\partial r}. \quad (4a)$$

In our previous publication (on a cylindrical geometry) (17), the left-hand side of the boundary condition at the capillary wall was inadvertently rendered as $P_{eff}c_p$, rather than $P_{eff}(c_p - c_i)$. The equation should have read:

$$P_{eff}(c_p - c_i) = -D \frac{\partial c_i}{\partial r} + V_i c_i, \quad (4b)$$

where V_i is the volume flow in the interstitium. This form had been used in calculations for publication. In the present paper, the convective term is omitted from Equation 4b, since it is assumed to be 0. Note also that sign conventions for the diffusive term are opposite for the cylindrical and spherical models. The boundary condition at the center of nodule, by symmetry, is:

$$D \frac{\partial c_i}{\partial r} = 0. \quad (4c)$$

This model treats diffusion from the nodule's surface to its center in one radial dimension, coupled with antigen-antibody interaction. The forward rate constant (k_f) and the corresponding reverse rate constant (k_r) for antigen-antibody interaction can be varied independently. Parameter values used for D , P_{eff} , and n are listed in Table 1. The affinity K_a (M^{-1}) is defined as k_f/k_r . Although k_f and k_r are taken arbitrarily for a series of calculations, these ranges are in agreement with the measurements of Dower et al. (24) and with the affinities determined by other investigators for many MABs. The antigen was assumed to be immobile and homogeneously distributed throughout the tumor, and individual cells were assumed to be small enough that they did not need to be modeled explicitly. Antigen concentration (expressed in terms of interstitial volume) was taken as $1 \mu M$, corresponding to $\sim 10^5$ antigens/cell, 10^9 cells/ml, and 17% extracellular space.

Calculation

The system of one partial and one ordinary differential equation describing this model was solved numerically by a computer program (which we term "PERC") based on the package PDECOL (25) that uses a collocation method for solution of the partial differential equations. Solutions were generated either on a VAX 8350 (Digital Equipment Co., Maynard, MA) or a CRAY XMP 24 (Cray Research Inc., Mendota Heights, MN).

The MAB concentration was calculated as a function of time and position in the tumor. Total MAB concentration at position i is the sum of free MAB and bound MAB:

$$\begin{aligned} c_{total,i} &= c_i + \bar{c} s_i \\ &= c_i + \frac{s_0 - s_i}{n}, \end{aligned} \quad (5)$$

where s_0 (M) is total antigen concentration at any point in the tumor (Table 1).

We also calculated an index of spatial nonuniformity (ISN), which indicates the inhomogeneity of radial MAB concentra-

TABLE 1
Parameter Values Used for the Baseline Calculation

Parameter	Baseline value
D effective interstitial diffusion coefficient	1.3×10^{-6} (cm ² /s)
P_{eff} effective capillary permeation constant	5.7×10^{-7} (cm/s) [†]
s_0 initial antigen concentration in tumor	1.0 (μM)
n valence of the MAB	2

^{*} This value is based on Ref. 27.

[†] Value approximately calculated by taking into account measured microvascular surface areas per unit volume, microvascular permeabilities, and nodule volumes (28-30)

tion throughout the tumor nodule at any given time (17):

$$ISN = \frac{\sqrt{\sum_{i=1}^N (c_i - \bar{c})^2}}{\sqrt{N(N-1)} \bar{c}}, \quad (6)$$

where \bar{c} is the mean of concentration throughout the tumor spheroid and N is the number of radial mesh points used in the numerical calculation. The mesh points correspond to thin, concentric, spherical shells. ISN ranges between 0 and 1. ISN = 0 indicates uniform distribution, and ISN = 1 indicates maximum nonuniformity (i.e., the case in which all MABs are located within one of the N spherical shells).

RESULTS

Effects of Affinity

The global pharmacokinetic parameters used for IgG after bolus i.v. injection are listed in Table 2. Figures 2-4 demonstrate the effects of affinity on MAB distribution from different points of view. The initial MAB plasma concentration was taken as 20 nM in these calculations. For the standard 70-kg person with a plasma volume of 3 liters, this initial MAB concentration corresponds to an injected bolus dose of ~ 9 mg of IgG.

Figure 2 shows microscopic MAB distribution profiles for different affinities ($K_a = 1.0 \times 10^7$, 1.0×10^8 , and $1.0 \times 10^9 M^{-1}$) up to 72 hr after injection. Lower MAB affinity leads to lower total concentrations near the surface of a nodule and higher total concentrations near the center than those calculated for higher affinity. Higher free (mobile) MAB concentration in tumor interstitium results in better percolation and less heterogeneous distribution. On the other hand, because the free MAB concentrations are lower (fewer mobile MAB), higher affinity MAB results in poor percolation and heterogeneous spatial distribution. Total concentration far from the surface is low.

Figure 3 shows the effect of varying K_a (from 1.0×10^7 to $1.0 \times 10^9 M^{-1}$) on total and free concentration at the surface, half-way to the center, and at the center of the tumor nodule. Free concentrations at all three sites are decreased as affinity increases (Fig. 3B). On the

other hand, the total concentration at these sites shows more complex behavior with increasing affinity (Fig. 3A). The total concentration adjacent to the surface of the nodule increases along with affinity, but the concentration at other sites first rises and then falls with increasing affinity.

Figure 4 shows the effect of varying K_a (over the same range as in Fig. 3) on the average total concentration and the ISN. Higher affinity leads to a higher average concentration. This relationship is significant in the lower affinity range. On the other hand, higher affinity leads to higher ISN (poor percolation, a more heterogeneous distribution), especially in the higher affinity range. Although high affinity leads to higher concentration adjacent to the surface of the nodule (i.e., MAb entry sites), the average antibody concentration in the tumor does not increase linearly with affinity and the contribution to the average total concentration is small in the higher affinity range. Thus, relatively low affinities (in the approximate range of 5×10^7 to 10^8 M^{-1}) are predicted to yield almost-maximal values of average

concentration without degrading the uniformity of distribution in this particular set of data.

Effects of Initial MAb Plasma Concentration

The initial MAb plasma concentrations were varied to analyze their effects on MAb distribution (Figs. 5 and 6). In these calculations, K_a was taken as $1.0 \times 10^9 \text{ M}^{-1}$ ($k_f = 1.0 \times 10^4 \text{ M}^{-1}\text{s}^{-1}$, $k_r = 1.0 \times 10^{-5} \text{ s}^{-1}$). Figure 5 shows microscopic MAb distribution profiles for the

TABLE 2
Parameter Values for Plasma MAb Pharmacokinetics*

	α_1	$\lambda_1 (\text{s}^{-1})$	α_2	$\lambda_2 (\text{s}^{-1})$
$^{111}\text{In-9.2.27}$	0.27	1.9×10^{-4}	0.73	7.4×10^{-6}

* Biexponential fit:

$$c_p = c_{p0} (\alpha_1 \cdot e^{-\lambda_1 t} + \alpha_2 \cdot e^{-\lambda_2 t}),$$
 where c_{p0} is initial MAb concentration.

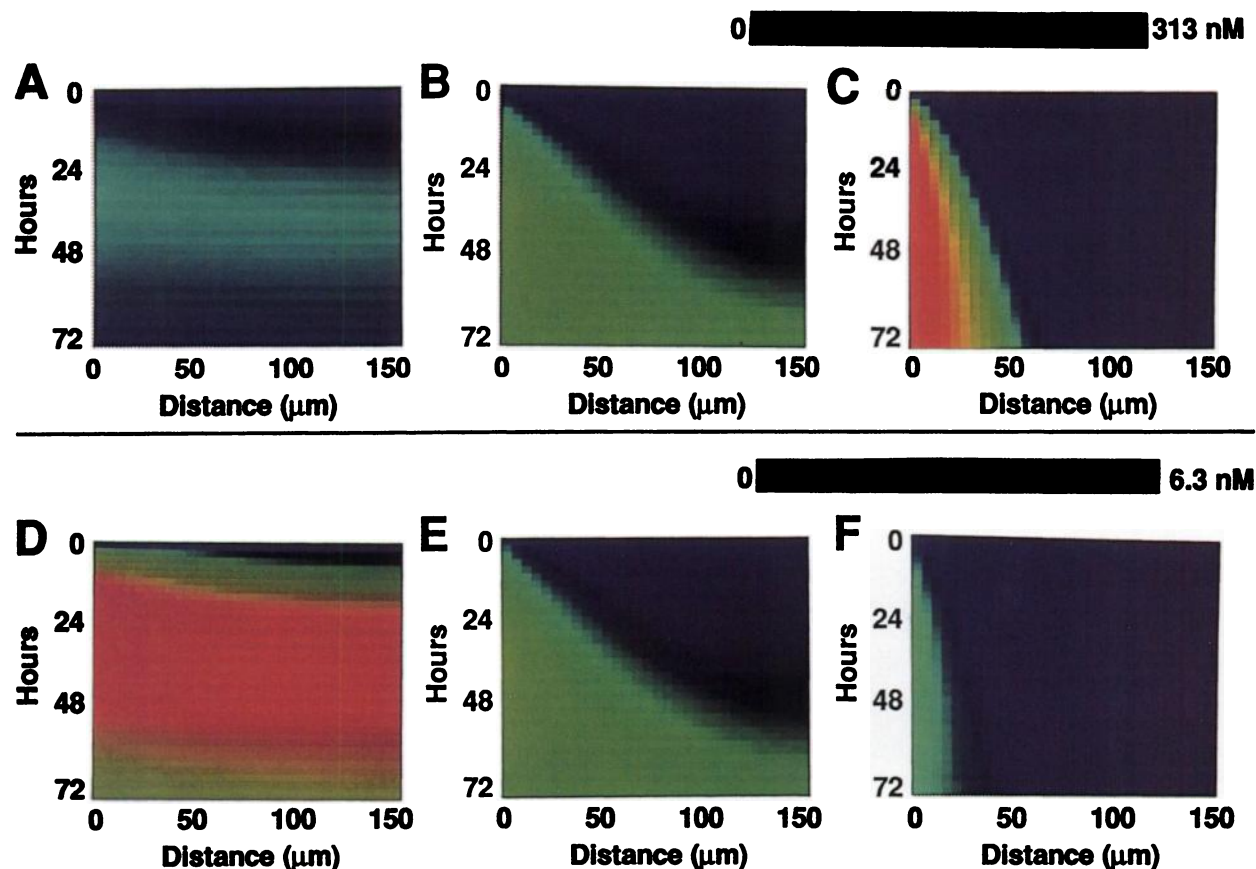


FIGURE 2

Total and free MAb distribution profiles of IgG: $K_a = 1.0 \times 10^7$ (A,D); $K_a = 1.0 \times 10^8$ (B,E); $K_a = 1.0 \times 10^9 \text{ M}^{-1}$ (C,F). Panels A–C: total MAb concentration; D–F: free MAb concentration. Color scale indicates MAb concentration. Note that the color scale of concentration in A–C is different from that in D–F. The horizontal axis indicates distance (μm) from the surface of the nodule. Thus, the distance $150 \mu\text{m}$ means the center of the nodule. The vertical axis indicates hours after i.v. bolus injection. Therefore, each horizontal stripe of color represents a computer-generated spatial profile of antibody concentration at a given point in time after the injection. Parameter values used other than K_a and the initial MAb plasma concentration are listed in Tables 1 and 2.

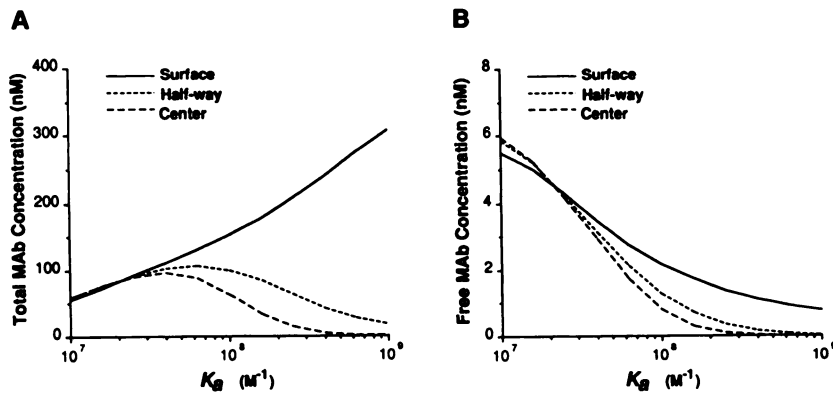


FIGURE 3
Effect of the antibody affinity (K_a) on total (A) and free (B) MAb concentration 48 hr after bolus injection. k_r was varied from 1.0×10^{-3} to $1.0 \times 10^{-5} \text{ s}^{-1}$ with k_f fixed as $1.0 \times 10^4 \text{ M}^{-1}\text{s}^{-1}$. Lines indicate concentrations just inside the surface of the nodule (—), half-way to the center (---), and at the center of the nodule (- - -).

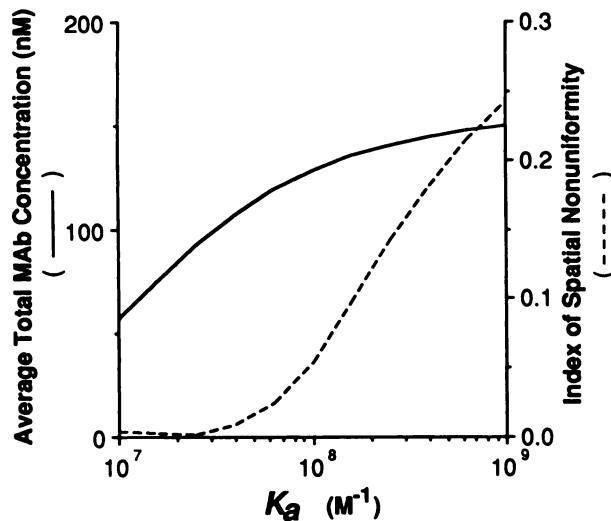


FIGURE 4
Effect of antibody affinity (K_a) on the average total MAb concentration (left y-axis; —) and the index of spatial nonuniformity (right y-axis; - - -) 48 hr after bolus injection. k_r was varied from 1.0×10^{-3} to $1.0 \times 10^{-5} \text{ s}^{-1}$ with k_f fixed $1.0 \times 10^4 \text{ M}^{-1}\text{s}^{-1}$.

different initial MAb plasma concentrations (10, 20, and 40 nM) up to 72 hr after i.v. injection. Higher initial MAb plasma concentration leads to both higher free and higher total MAb concentrations in tumor interstitium. Even though total MAb concentrations near the nodule's surface do not linearly relate to the initial MAb plasma concentration, higher initial MAb plasma concentration results in better percolation through tumor interstitium.

Figure 6 shows the effect of varying the initial MAb plasma concentration (from 10 to 100 nM) on the average total concentration and the ISN. Higher initial MAb plasma concentration leads to a higher average total concentration and lower ISN (better percolation, a more homogeneous distribution). Because of binding-site saturation, average total MAb concentration does not linearly relate to the initial MAb plasma concentration in higher dose ranges ($\geq 70 \text{ nM}$ in this particular set of data). ISN dramatically decreases in this range.

Interaction of Initial MAb Plasma Concentration and the Affinity

Figures 7A-B show the effect of varying the initial MAb plasma concentration (from 10 to 100 nM) and K_a (from 1.0×10^7 to $1.0 \times 10^9 \text{ M}^{-1}$) on the average total concentration (Fig. 7A) and ISN (Fig. 7B).

Increasing both the initial MAb plasma concentration and K_a increased the average total concentration in tumor (Fig. 7A). However, their contributions to the average total concentration are not same. For example, a two-fold increase in the initial MAb plasma concentration (20 to 40 nM) results in 1.84-, 1.90-, and 1.92-fold increase in average total concentration for $K_a = 1.0 \times 10^7$, 1.0×10^8 , and $1.0 \times 10^9 \text{ M}^{-1}$, respectively. On the other hand, even a ten-fold increase of affinity results in only a 2.25-fold increase in average total concentration for $K_a = 1.0 \times 10^7$ to 1.0×10^8 and a 1.17-fold increase for $K_a = 1.0 \times 10^8$ to 1.0×10^9 (with 20 nM initial MAb plasma concentration).

The relationship between increasing dose and increasing affinity in terms of ISN as a response variable is indicated Figure 7B. Increasing affinity K_a results in increased ISN, especially in the higher affinity range with lower initial MAb plasma concentration (Fig. 7B). For 20 nM initial MAb plasma concentration, a ten-fold increase in K_a (from 1.0×10^7 to 1.0×10^8) results in a 14.3-fold increase in the ISN, and a 100-fold increase in K_a (from 1.0×10^7 to 1.0×10^9) results in a 64.3-fold increase in the ISN. Average total concentration increases only 2.25-fold and 2.63-fold, respectively.

DISCUSSION

We have examined the effect of MAb affinity and demonstrated the relationship between affinity and MAb distribution in a hypothetical tumor nodule.

Antibodies have the advantage of selective binding to specific sites. The most important prediction by this model is that antigen-antibody interaction in the tumor nodule imposes a binding-site barrier that retards MAb percolation and causes a heterogeneous distribution. The higher the affinity of binding, the fewer free mole-

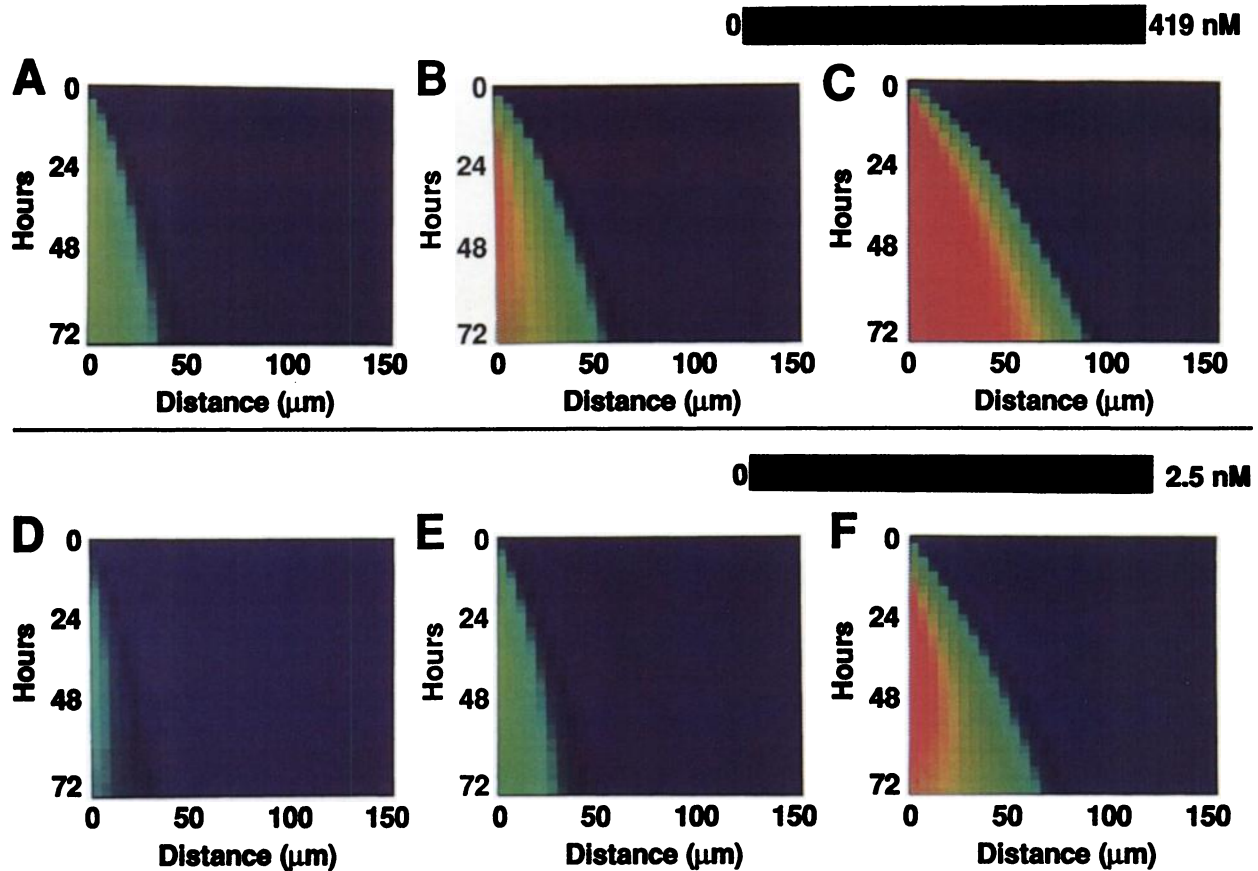


FIGURE 5

Total and free MAb distribution profiles of IgG after bolus i.v. injection. Initial MAb plasma concentration 10 nM (A,D); 20 nM (B,E); and 40 nM (C,F). Panels A–C: total MAb concentration; D–F: free MAb concentration. Note that the color scale of concentration in A–C is different from that in D–F. The horizontal axis indicates distance (μm) from the surface of the nodule. The vertical axis indicates hours after i.v. bolus injection. Therefore, each horizontal stripe of color represents a computer-generated spatial profile of antibody concentration at a given point in time after the injection. Parameter values used other than the initial MAb plasma concentration and K_a (taken as $1.0 \times 10^9 \text{ M}^{-1}$) are listed in Tables 1 and 2.

cules there will be (all else being equal) to penetrate farther into the tumor interstitium. Hence, there is a tendency for high affinity (high k_f , low k_r) to decrease the uniformity of MAb distribution. High affinity leads to higher concentration near entry sites but does not greatly increase the average concentration (Figs. 3 and 4). Without specific binding, however, the concentration of MAb would rise no higher than the plasma concentration, so too low an affinity would clearly not be useful. These general principles hold also for model geometries representing flux of MAb away from a vascular surface in Cartesian coordinates (13–15,26) and representing outward flux from a central blood capillary in cylindrical cords of tumor cells (17). These models show a similar relationship between MAb concentration and affinity, although they are quantitatively different. In the spherical model, MAb transport is converging, whereas, it is diverging in a cylindrical model. Generally, the “binding barrier problem” for those sites far from entry points may be more significant in a cylindrical model.

One strategy to overcome the binding-site barrier would be to increase the initial MAb dose. Even though MAb concentration in tumor does not always increase linearly as initial MAb plasma concentration increases, a high initial plasma concentration leads to better percolation and results in more uniform distribution in tumor (Figs. 5 and 6). Increasing MAb dose, however, decreases the specificity ratio (tumor/nontumor ratio, or tumor/plasma ratio) (17) and may cause toxicity or other side effects. For each MAb species and set of circumstances, there is an inherent balance of factors. Other causes of heterogeneous distribution include the functional and anatomical heterogeneity of tumors and their vessels, as studied by Dvorak et al. (9), and the elevated interstitial pressures analyzed by Jain and Baxter (27).

For diagnostic imaging, microscopic distribution is expected to be a secondary issue as compared with the average concentration in a macroscopic region of tumor. If the aim of therapy with an antibody-conjugated alpha emitter were to damage the tumor’s blood vessels

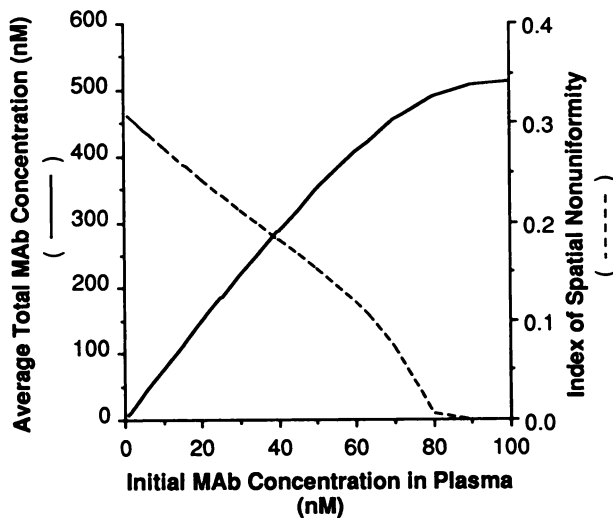


FIGURE 6
Effect of initial MAb plasma concentration on the average total MAb concentration (left y-axis; —) and the index of spatial nonuniformity (right y-axis; - - -) 48 hr after bolus injection. Initial MAb plasma concentration was varied from 1 to 100 nM. k_r was taken as $1.0 \times 10^{-5} \text{ s}^{-1}$ and k_f as $1.0 \times 10^4 \text{ M}^{-1}\text{s}^{-1}$ ($K_a = 1.0 \times 10^9 \text{ M}^{-1}$). The striking behavior near 80 nM initial concentration is a true reflection of the physical chemistry, not a numerical artifact.

and immediately surrounding cells, poor percolation might be an advantage; if, on the other hand, the aim were to reach all tumor cells, including those distant from the vascular supply, poor percolation would be a significant problem. Given the set of parameter values used for the calculations in Figures 2-4, the affinity can be decreased to approximately $5 \times 10^7 \text{ M}^{-1}$ to achieve uniform distribution without significant decrease in the average concentration (Fig. 4). This model therefore

suggests the existence of a range of parameter values in which lower affinity can improve percolation at a given dose with only a moderate decrease in the average concentration. This range depends, of course, on the other parameter values (e.g., MAb dose, antigen concentration, vascular permeation rate) and other factors (e.g., metabolism of MAb-conjugates) (17).

We have considered here the problem of a binding-site barrier. This modeling analysis predicts a set of complex trade-offs (Fig. 7): antibody affinity and dose optimized for radioimmuno-detection may not be favorable for radioimmunotherapy intended to kill the last tumor cell.

The calculations presented here must be considered as predictions from a mathematically abstract case. There is clearly a great deal of variability in tumor vascular patterns and tumor histology. No single model can be expected to capture all of the salient elements of tumor architecture, and this model (as well as the cylindrical one described elsewhere (17)) should be considered as providing reasonable constructs for thinking about the problem. These calculation reinforce the idea that a complex interplay of factors must be considered in the design of next-generation molecules and methods. These models and concepts are quite general in form: the global pharmacokinetics, transcapillary transport, percolation, binding kinetics, and cellular metabolism can be specified (and modeled using PERC) for macromolecular ligands other than immunoglobulins, and also for low molecular weight species. It should be noted as well that the spatial distributions calculated using PERC can be combined with information on the microdosimetry of any given isotope to calculate the distribution of radiation dose within a tumor.

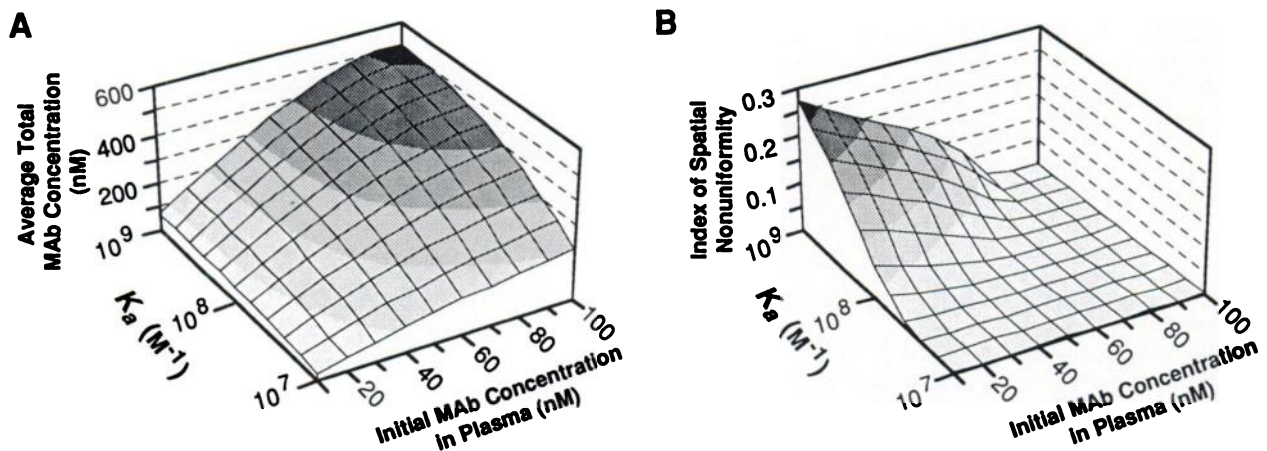


FIGURE 7
Effect of initial MAb plasma concentration and K_a on the average total MAb concentration (A) and ISN (B) 48 hr after bolus injection. Initial MAb plasma concentration was varied from 10 to 100 nM. k_r was varied from 1.0×10^{-5} to $1.0 \times 10^{-3} \text{ s}^{-1}$ with k_f as $1.0 \times 10^4 \text{ M}^{-1}\text{s}^{-1}$ (thus, K_a was varied from 1.0×10^7 to $1.0 \times 10^9 \text{ M}^{-1}$). These graphs show the interaction between initial MAb concentration and K_a .

ACKNOWLEDGMENTS

The authors acknowledge the National Cancer Institute for allocation of computing time and staff support at the Advanced Scientific Computing Laboratory of the Frederick Cancer Research Facility. The authors thank Kai-Li Ting, PhD, for programming the color graphic output.

REFERENCES

1. Abrams PG, Oldham RK. Monoclonal antibody therapy of solid tumors. In: Foon KA, Morgan AC Jr., eds. *Monoclonal antibody therapy of human cancer*. Boston, MA: Martinus Nijhoff; 1985;103-120.
2. Meeker TC, Lowder J, Maloney DG, et al. A clinical trial of anti-idiotypic therapy for B cell malignancy. *Blood* 1985; 65:1349-1363.
3. Jones PL, Gallagher BM, Sands H. Autoradiographic analysis of monoclonal antibody distribution in human colon and breast tumor xenografts. *Cancer Immunol Immunother* 1986; 22:139-143.
4. Sands H, Jones PL, Shah SA, Palme D, Vessella RL, Gallagher BM. Correlation of vascular permeability and blood flow with monoclonal antibody uptake by human Clouser and renal cell xenografts. *Cancer Res* 1988; 48:188-193.
5. Dedrick RL, Flessner MF. Pharmacokinetic considerations on monoclonal antibodies. In: Mitchell M, ed. *Immunity to Cancer II: proceedings of 2nd conference on immunity to cancer*. New York: Alan R. Liss; 1989:429-438.
6. Schlom J, Colcher D, Hand PH, Wunderlich D, Nuti M, Teramoto YA. Antigenic heterogeneity, modulation and evolution in breast cancer lesions as defined by monoclonal antibodies. In: Rich M, Hager JC, Furmanski P, eds. *Understanding breast cancer: clinical and laboratory concepts*. New York: Marcel Dekker, Inc.; 1983:315-358.
7. Del Vecchio S, Reynolds JC, Blasberg RG, et al. Measurement of local Mr 97,000 and 250,000 protein antigen concentration in sections of human melanoma tumor using in vitro quantitative autoradiography. *Cancer Res* 1988; 48:5475-5481.
8. Jain RK. Determinants of tumor blood flow: a review. *Cancer Res* 1988; 48:2641-2658.
9. Dvorak HF, Nagy JA, Dvorak JT, Dvorak AM. Identification and characterization of the blood vessels of solid tumors that are leaky to circulating macromolecules. *Am J Pathol* 1988; 133:95-109.
10. Eger RR, Covell DG, Carrasquillo JA, et al. Kinetic model for the biodistribution of an ¹¹¹In-labeled monoclonal antibody in humans. *Cancer Res* 1987; 47:3328-3336.
11. Covell DG, Barnet J, Holton OD III, Black CDV, Parker RJ, Weinstein JN. Pharmacokinetics of monoclonal immunoglobulin G1,F(ab')₂, and Fab' in mice. *Cancer Res* 1986; 46:3969-3978.
12. Holton OD III, Black CDV, Parker RJ, et al. Biodistribution of monoclonal IgG₁, F(ab')₂, and Fab' in mice after intravenous injection: a comparison between anti-B cell (anti-LyB8.2) and irrelevant (MOPC-21) antibodies. *J Immunol* 1987; 139:3041-3049.
13. Weinstein JN, Black CDV, Barbet J, et al. Selected issues in the pharmacology of monoclonal antibodies. In: Tomlinson E, David SS, eds. *Site-specific drug delivery*. New York: John Wiley & Sons; 1986:81-91.
14. Weinstein JN, Eger RR, Covell DG, et al. The pharmacology of monoclonal antibodies. *Ann NY Acad Sci* 1987; 507:199-210.
15. Weinstein JN, Covell DG, Barbet J, et al. Local and cellular factors in the pharmacology of monoclonal antibodies. In: Bonavida B, Collier RJ, eds. *Membrane mediated toxicity*. New York: Alan R. Liss; 1987:279-289.
16. Fujimori K, Weinstein JN. Pharmacokinetics and organ targeting of monoclonal antibodies. In: Hadden JW, Spreafico F, Yamamura Y, Austen KF, Dukor P, Masek K, eds. *Advances in immunopharmacology, Vol. 4*. Oxford, England: Pergamon Press; 1989:127-129.
17. Fujimori K, Covell DC, Fletcher JE, Weinstein JN. Modeling analysis of the global and microscopic distribution of IgG, F(ab')₂, and Fab in tumors. *Cancer Res* 1989; 49:5656-5663.
18. Sutherland RM. Cell and environment interactions in tumor microregions: the multicell spheroid model. *Science* 1988; 240:177-184.
19. Crank J. *The mathematics of diffusion*. Oxford, England: Oxford University Press; 1975:69.
20. Rubin P, Casarett G. Microcirculation of tumors part I: anatomy, function, and necrosis. *Clin Radiol* 1966; 17:220-229.
21. Langmuir VK, McGann JK, Buchegger F, Sutherland RM. ¹³¹I-anticarcinoembryonic antigen therapy of LS174T human colon adenocarcinoma spheroids. *Cancer Res* 1989; 49:3401-3406.
22. McFadden R, Kwok C. Mathematical model of simultaneous diffusion and binding of antitumor antibodies in multicellular human tumor spheroids. *Cancer Res* 1988; 48:4032-4037.
23. Nakagawa H, Groothuis DR, Owens ES, Fenstermacher JD, Patlak CS, Blasberg RG. Dexamethasone effects on [¹²⁵I] albumin distribution in experimental RG-2 gliomas and adjacent brain. *J Cereb Blood Flow Metab* 1987; 7:687-701.
24. Dower SK, Ozato K, Segal DM. The interaction of monoclonal antibodies with MHC class I antigens on mouse spleen cells. I. Analysis of the mechanism of binding. *J Immunol* 1984; 132:751-758.
25. Madsen NK, Sincovec RF. Algorithm 540 PDECOL, general collocation software for partial differential equations [D3]. *ACM Trans Math Software* 1979; 5:326-351.
26. Weinstein JN, Black CDV, Holton OD III, et al. Delivery of monoclonal antibodies to lymph nodes via the lymphatics. In: Holcenberg JS, Winkkelhake JL, eds. *The pharmacology and toxicology of proteins*. New York: Alan R. Liss, Inc.; 1987:75-89.
27. Jain RK, Baxter LT. Mechanisms of heterogeneous distribution of monoclonal antibodies and other macromolecules in tumors: significance of elevated interstitial pressure. *Cancer Res* 1988; 48:7022-7032.
28. Gerlowski LE, Jain RK. Microvascular permeability of normal and neoplastic tissues. *Microvasc Res* 1986; 31:288-305.
29. Hilmas D, Gilette EL. Morphometric analyses of the microvasculature of tumors during growth and after X-irradiation. *Cancer* 1974; 33:103-110.
30. Yamamura H, Sato H. Quantitative studies on the developing vascular system of rat hepatoma. *J Natl Cancer Inst* 1974; 53:1229-1240.